Electron spin resonance and electron nuclear double resonance of photogenerated polarons in polyfluorene and its fullerene composite

K. Marumoto,* M. Kato, H. Kondo, and S. Kuroda
Department of Applied Physics, Graduate School of Engineering, Nagoya University, Chikusa-ku, Nagoya 464-8603, Japan

N. C. Greenham and R. H. Friend
Cavendish Laboratory, University of Cambridge, J. J. Thomson Avenue, Cambridge CB3 0HE, United Kingdom

Y. Shimoi and S. Abe
Nanotechnology Research Institute (NRI), National Institute of Advanced Industrial Science and Technology (AIST), Tsukuba, Ibaraki 305-8568, Japan

(Received 17 April 2009; published 18 June 2009)

Electron spin resonance (ESR) and electron-nuclear double resonance (ENDOR) of photogenerated polarons in poly(9,9-dioctylfluorene) (PFO) and its composite with fullerene (C_{60}) using variable photoexcitation energy up to 4.1 eV are reported. For PFO, a light-induced ESR (LESR) signal ($g=2.003$) is observed below 60 K, and its transient response and excitation spectrum indicate that the observed spins are photogenerated polarons on PFO. For the PFO-C_{60} composite, two LESR signals of photogenerated positive polarons on PFO ($g_1=2.003$) and radical anions on C_{60} ($g_2=1.999$), respectively, are observed below 120 K, which are caused by photoinduced electron transfer from PFO to C_{60}. A remarkable enhancement of the LESR signals in the excitation spectrum at ~2.8 eV is observed compared with the case of pure PFO. The bimolecular-recombination kinetics of photogenerated charge carriers in the composite are confirmed by the dependence of the LESR on excitation-light intensity and by the decay dynamics. Light-induced ENDOR (LENDOR) signals are clearly observed for excitation around 2.8 eV owing to the highly efficient photoinduced electron transfer in the composite. Broad LENDOR shifts directly reflect the spin-density distribution of the polarons in PFO. We have determined its maximum shift using LENDOR-induced ESR, and have evaluated the maximum spin density on the carbon site coupled to the proton as 0.032. This value is consistent with the theoretical result obtained by Pariser-Parr-Pople (PPP) model, where the spatial extent of the polarons is calculated as ~3 monomer units of PFO. The calculated LESR spectra of PFO based on the PPP model are consistent with the experimental spectra, which confirm the above spatial extension of the polaron in PFO.

DOI: 10.1103/PhysRevB.79.245204 PACS number(s): 81.05.Lg, 76.30.−v

I. INTRODUCTION

Quasi-one-dimensional conducting conjugated polymers have been investigated extensively because of a wide variety of interesting physical properties such as electroluminescence, nonlinear optical effects, and semiconductor-metal transitions.[1–3] Among conducting polymers, poly(9,9-dioctylfluorene) (PFO) has attracted much attention because light-emitting diodes (LEDs) of PFO show highly efficient blue electroluminescence.[4–10] Photoinduced charge separation in polymeric semiconductors is important, because its study not only contributes to understanding of the basic photoexcited states in these one-dimensional semiconductors, but also contributes to the development of efficient nonlinear optical and photovoltaic devices.[11] Composites of conducting polymers such as poly(3-alkylthiophene) (P3AT), poly(*p*-phenylenevinylene) (PPV) derivatives and PFO, and high-electron affinity species such as fullerene (C_{60}) and C_{60} derivatives have been investigated extensively, because highly efficient photoinduced charge separation occurs in the polymer-C_{60} composites upon C_{60} doping, which is useful to develop the efficient nonlinear optical and photovoltaic devices.[12–25] This charge separation is attributed to photoinduced electron transfer from polymer to C_{60}, which forms positive charges on polymer chains and radical anions of C_{60} molecules, respectively. The positive charge carriers on conjugated polymers are considered to be polarons,[1] however, the nature of the polaronic states has not yet been completely clarified.

Electron spin resonance (ESR) is capable of directly observing paramagnetic species such as polarons. In particular, light-induced ESR (LESR) is a direct microscopic method for detecting and studying the photogenerated polarons and has been employed to clarify the polaronic states in PPV and its derivatives,[26–33] oligothiophenes,[34] and regioregular poly(3-alkylthiophene) (RR-P3AT) using its composites with C_{60}.[35–42] The LESR studies have clarified the mechanism of the charge separation and recombination of the photogenerated carriers in these materials. Moreover, the ESR method with the aid of electron-nuclear double resonance (ENDOR) technique can evaluate the spatial extent of polarons in the polymers; the spatial extents of polarons in PPV and RR-P3AT have been evaluated as four PPV monomer units and ten thiophene monomer units, respectively, from the spin-density distribution of polarons. This ESR method has also evaluated the spatial extent of field-injected charge carriers in pentacene as being on the order of 10 molecules using field-effect transistors; pentacene is a typical organic oligomeric semiconductor.[43] For PFO and its composite with C_{60}, however, the LESR study has not yet been performed. This

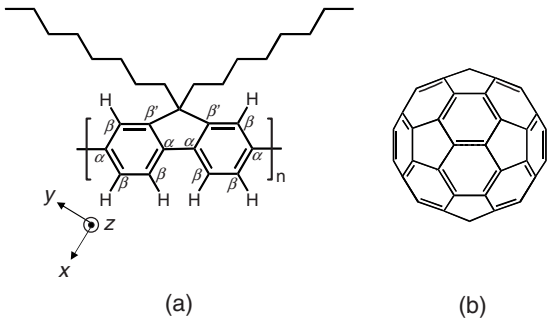

FIG. 1. Chemical structures of (a) poly(9,9-dioctylfluorene) (PFO) and (b) fullerene (C_{60}). In (a), principal axes of proton-hyperfine coupling of a π electron are shown. α, β, and β' define the sites of α, β, and β' carbons, respectively.

study would provide important information on the spatial extent of polarons as well as the mechanism of the charge separation and recombination of the photogenerated carriers in the blue-electroluminescent polymer PFO.

In this paper, we report on the LESR studies of the PFO-C_{60} composite in addition to the pure PFO using variable photoexcitation energy. A remarkable enhancement of the LESR signals of the composite in excitation spectrum is observed compared with the case of the pure PFO at around 2.8 eV owing to photoinduced charge separation. Using a light-induced ENDOR (LENDOR) technique and a theoretical calculation within the Pariser-Parr-Pople (PPP) model, the spatial extent of photogenerated polarons in PFO has been evaluated as ~3 PFO monomer units. The calculated ESR spectra based on the PPP model have successfully reproduced the experimentally obtained LESR spectra, which have confirmed the above spatial extent of polarons. The paper is organized as follows: after describing the experimental procedure in Sec. II, we present the LESR study of the pure PFO in Sec. III A. Second, the LESR study of the PFO-C_{60} composite is presented in Sec. III B. Next, we present the LENDOR study of the PFO-C_{60} composite in Sec. III C. Finally, we present the theoretical analysis of polarons in PFO in Sec. III D. We summarize our results in Sec. IV.

II. EXPERIMENTAL PROCEDURE

PFO was synthesized as described in the literature [Fig. 1(a)].[4–10] The powder sample of PFO (15 mg) was inserted into an ESR sample tube and then sealed under vacuum condition below 10^{-4} Pa. PFO was used to prepare the PFO-C_{60} composite (Fig. 1). The concentration of C_{60} was 5% for a PFO repeat unit (PFO:C_{60}=1:0.093 by weight ratio). Ultrasonic treatment of PFO-C_{60} toluene solution was carried out with an ultrasonic disintegrator for better uniform mixing. Cast films of the PFO-C_{60} composite were fabricated on polyethylene-terephthalate substrates under argon-gas atmosphere, which were inserted into ESR sample tubes and then sealed under vacuum condition below 10^{-4} Pa. ESR measurements were performed with a Bruker E500 X-band spectrometer with a microwave cavity with optical windows down to liquid-helium temperature using an Oxford ESR900 gas-flow cryostat. The absolute magnitude of the g value was calibrated utilizing an NMR gauss meter for obtaining the static magnetic field strength and a microwave frequency counter. A JASCO SM-5 light source with a 300 W xenon lamp was used to provide excitation for 300–1100 nm (1.1–4.1 eV) at power levels up to 2 mW/cm^2 with a spectral width of 10 nm. The light was delivered by an optical fiber to the quartz sample tube. For the excitation spectrum, the light intensity was adjusted to give the same photon flux at each wavelength.

The LESR experimental procedure consisted of the following sequence: (i) scan the ESR spectrum of the nonilluminated sample; (ii) scan the ESR spectrum under light illumination; (iii) turn off the illumination and scan the ESR spectrum; and (iv) warm the sample up to room temperature, cool it down to working temperature, and scan the ESR spectrum again. These ESR signals will be referred to as: "dark," "light-on," "light-off," and "annealed" signals, respectively. As discussed below, the switching off of the excitation light does not lead to the disappearance of the ESR signals at low temperature. To eliminate the ESR spectrum completely, the sample had to be warmed up to room temperature (annealing). This step was performed every time while measuring the dependences of the temperature, microwave power, excitation-light energy, and excitation-light intensity. The dark and annealed ESR signals were confirmed to be the same as each other every time. As default definition of the term LESR we choose the light-on signal corrected by subtracting the dark signal. Finally, we distinguish between the prompt LESR signal (light-on minus light-off) and the persistent one (light-off minus dark).

III. RESULTS AND DISCUSSION

A. LESR of PFO

First, we present the results of the pure PFO. Upper curves in Fig. 2 show the observed first-derivative ESR spectra of the PFO under dark conditions (dotted line) and 300 nm illumination (solid line) at 10 K with a microwave power of 0.06 mW where no saturation occurs. The lower curve in Fig. 2 shows the LESR spectrum obtained by subtracting the ESR spectrum under dark conditions from that under 300 nm illumination. The g value is obtained as g=2.003. The observed spins in the dark condition might be attributed to the trapped polarons, possibly generated by oxygen doping or chemical defects, as observed in PPV,[26] oligothiophenes,[34] and RR-P3AT.[35,38] The LESR intensity is approximately five times as large as the dark ESR intensity. The LESR spectrum has an almost symmetric line shape. The spin concentration obtained from the LESR signal is evaluated as one spin per 3.5×10^7 PFO-repeat units, which is much lower than that obtained for RR-P3AT.[35] The peak-to-peak linewidth (ΔH_{pp}) of the LESR signal of PFO is approximately 3.0 G. The LESR signal of PFO becomes undetectable above approximately 60 K owing to the higher recombination rate, confirming that the LESR signal is transient in nature.[30,32,35] The temperature dependence of the LESR intensity is similar to that of the RR-P3AT and the RR-P3AT-C_{60} composite.[35] The

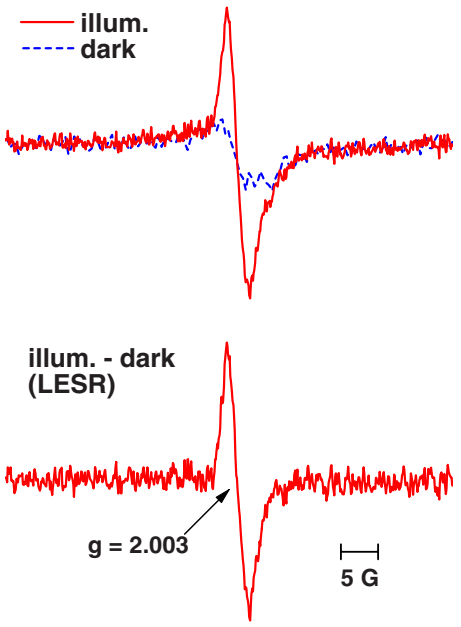

FIG. 2. (Color online) Upper curves: ESR spectra of PFO under dark conditions (dotted line) and 300 nm illumination (solid line) at 10 K. Lower curve: LESR spectrum of PFO obtained by subtracting the dark spectrum from that under 300 nm illumination at 10 K.

ΔH_{pp} of the LESR signal does not depend on the temperature at which the signals were measured.

The excitation spectrum of the LESR signal provides important information concerning the mechanism of the photogeneration of polarons. Figure 3 shows the variation in the normalized peak-to-peak LESR intensity (I_{pp}) with the photon energy of the incident light for the PFO. The measurements were performed with a microwave power of 0.06 mW at 10 K. For comparison, the reported optical absorption[10] and photocurrent action spectra[7] of the PFO are shown together in Fig. 3. The absorption measurement was performed at room temperature using a semicrystalline film.[10] The photocurrent action spectrum was measured using a sandwich-structure device with an indium-tin-oxide (ITO) anode and

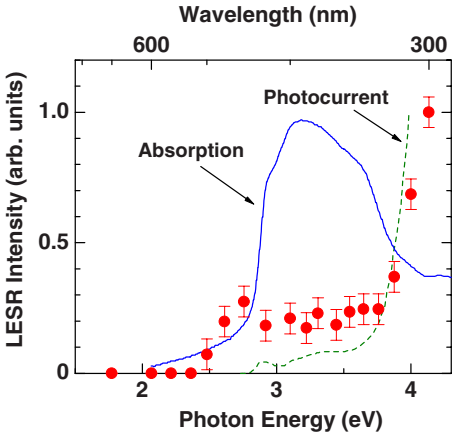

FIG. 3. (Color online) Excitation spectrum of the LESR signal of PFO at 10 K (solid circles). The solid line shows the absorption spectrum of the crystalline film of PFO. The dotted line shows the photocurrent action spectrum of PFO.

an aluminum cathode.[7] The excitation spectrum of the LESR signal shows a rapid increase above ~3.7 up to 4.1 eV, despite the lower optical density, as observed in PPV and its derivatives and in RR-P3AT.[29–32,35] Similar behavior with a threshold of ~3.6 eV has been also observed for the action spectrum of photocurrent, as shown in Fig. 3.[7] This behavior indicates that the observed spins are photogenerated polarons whose generation efficiency increases above the optical-absorption peak due to excitons, because weakly bound electrons and holes created can be more readily dissociated into polarons. It is interesting to note that the energy difference between the single-particle highest occupied molecular-orbital (HOMO) level and the lowest unoccupied molecular-orbital (LUMO) level of PFO has been estimated as 3.55 ~3.68 eV by using x-ray photoelectron spectroscopy (XPS) and cyclic voltammetry measurements.[6,8] The energy is consistent with the threshold energy obtained from the rapid increase in the LESR intensity, which indicates that the threshold energy of LESR corresponds to the single-particle band gap of PFO, that is, or the energy difference between HOMO and LUMO levels. For other energy regions, there is an increase in the LESR intensity at around 2.8 eV (450 nm). The LESR spectral line shape at 450 nm almost agrees with that at 300 nm, suggesting that the light-induced spin species are also polarons. Even with low-photon energy, charge separation such as electron transfer between molecules and oxygen or other defects may occur. Similar increases have been observed in PPV,[29] oligothiophenes,[34] and RR-P3AT.[35]

B. LESR of the PFO-C_{60} composite

Second, we present the results of the PFO-C_{60} composite. Upper curves in Fig. 4 show the observed first-derivative ESR spectra of the PFO-C_{60} composite under dark conditions (dotted line) and 450 nm illumination (solid line) at 10 K with a microwave power of 0.06 mW where no saturation occurs. The lower curve in Fig. 4 shows the LESR spectrum obtained by subtracting the ESR spectrum under dark conditions from that under 450 nm illumination. Two LESR signals due to the photoinduced electron transfer from PFO to C_{60} are observed. The obtained g values of $g_1=2.003$ and $g_2=1.999$ correspond to the positive polarons on PFO and radical cations C_{60}^-, respectively, as similarly observed in the LESR studies of the RR-P3AT-C_{60} composites.[35–42] The observed polaron spins under dark conditions are considered to be attributed to the trapped polarons mentioned above in the discussion of the pure PFO. The LESR intensity is approximately three times as large as the dark ESR intensity. The dark ESR and LESR spectra seem to be slightly different to each other because of the overlapping of the LESR signals of PFO and C_{60}. Since the LESR signals of PFO (g_1) and C_{60} (g_2) overlap with each other, it is difficult to obtain a precise half-amplitude linewidth ($\Delta H_{1/2}$) from the experimental result directly. Hereafter, we define each peak-to-peak linewidth (ΔH_{pp}) of the LESR signals of PFO and C_{60} as an interval of the magnetic field between a maximum and a minimum of the first-derivative LESR spectrum around g_1 and g_2, respectively. The ΔH_{pp} of the LESR signals of PFO and C_{60} are approximately 2.1 and 2.6 G, respectively. A

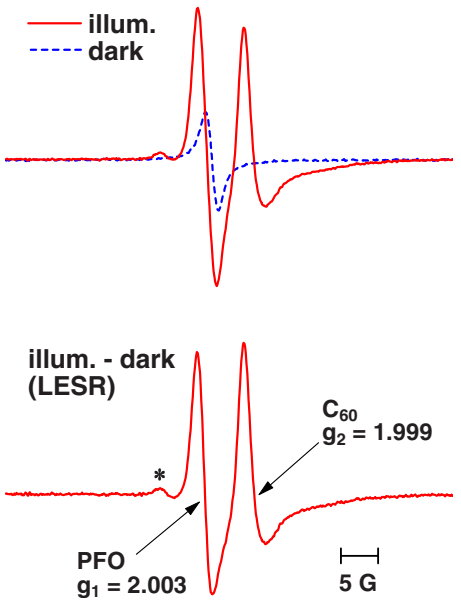

FIG. 4. (Color online) Upper curves: ESR spectra of the PFO-C_{60} composite (C_{60}:5%) under dark conditions (dotted line) and 450 nm illumination (solid line) at 10 K. Lower curve: LESR spectrum of the PFO-C_{60} composite obtained by subtracting the dark spectrum from that under 450 nm illumination at 10 K. The weak signal in the lower magnetic field region denoted by an asterisk (*) is the so-called spin-flip transition.

weak signal has been observed in the region of lower magnetic field, denoted by an asterisk (*) in Fig. 4. This signal is ascribed to the resonance of forbidden transition due to nuclear spins of hydrogen at low temperatures and is known as a spin-flip transition; this phenomenon has been also observed in PPV.[28]

Figure 5 shows the temperature dependence of the LESR intensity of the PFO-C_{60} composite. The solid circles and open squares denote the peak-to-peak amplitude intensity (I_{pp}) of LESR signals of PFO (g_1) and C_{60} (g_2), respectively. The data were recorded with a microwave power of 0.06 mW under 450 nm illumination. The ΔH_{pp} of the LESR signals does not depend on the temperature, except for the low-temperature region of 4 K where the saturation occurs. The

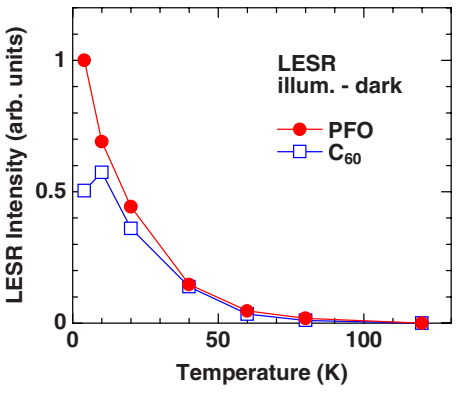

FIG. 5. (Color online) Temperature dependence of the LESR intensities of the PFO-C_{60} composite. The solid circles and open squares denote the signal intensities of PFO and C_{60}, respectively.

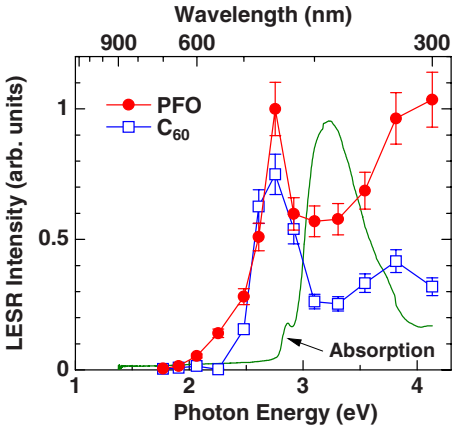

FIG. 6. (Color online) Excitation spectra of the LESR signals of the PFO-C_{60} composite (C_{60}:5%) at 10 K. Solid circles and open squares denote the signal intensities of PFO and C_{60}, respectively. The solid line shows the absorption spectrum of the PFO-C_{60} composite (C_{60}:5%) for the comparison.

LESR signals become undetectable above approximately 120 K due to the higher recombination rate, confirming that the LESR signals are transient in nature.[30,32,35] The decrease in the signal at low temperature is caused by saturation of the ESR signals due to the longer spin-lattice relaxation rate.

The excitation spectrum of the LESR signals of the PFO-C_{60} composite is shown in Fig. 6, which presents the variation in the normalized I_{pp} with the photon energy of the incident light for the PFO-C_{60} composite. The measurements were performed with a microwave power of 0.06 mW at 10 K. For comparison, the absorption spectrum (solid line) of the PFO-C_{60} composite measured using a cast film is shown in Fig. 6. The excitation spectrum of the LESR signals of PFO (g_1) shows a noticeable enhancement at around 2.8 eV (450 nm), which is probably caused by the photoinduced electron transfer following absorption in the weakly allowed C_{60} transition ($h_u \rightarrow t_{1u}$) at this energy. We note also that the profile of absorption through the thickness of the film is rapidly changing at near threshold of absorption for the PFO; absorption of light within the bulk of the film is large when the optical density of the film is near unity, but falls at higher photon energy as light is absorbed primarily near the surface of the film. This may also contribute to the peak in response near 2.8 eV if there were a variation in concentration of C_{60} between bulk and surface. The excitation spectrum of the LESR signals of C_{60} (g_2) shows a similar behavior to that of PFO. There is no excitation-energy dependence of the LESR line shapes, which confirms the observation of same polarons in PFO. The enhancement at around 2.8 eV is clearly shown by comparing the LESR excitation spectrum of the PFO-C_{60} composite with that of the pure PFO shown in Fig. 3. There is a slight difference between the excitation spectra of the PFO and C_{60} resonances; a monotonic increase above 3 up to 4.1 eV is observed for PFO (g_1) while another peak at around 3.8 eV is observed for C_{60} (g_2). One possible explanation for this difference is the direct formation of photogenerated polarons in PFO without the photoinduced electron transfer from PFO to C_{60} mentioned above. The measurement of photocurrent action spectrum of the PFO-C_{60} com-

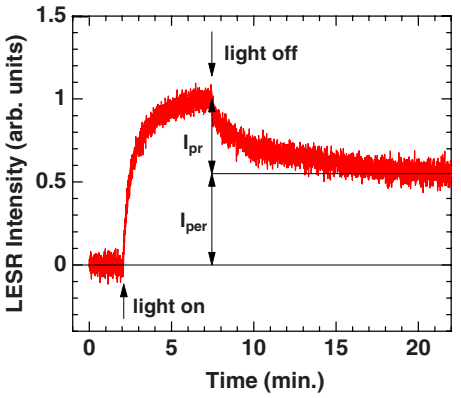

FIG. 7. (Color online) Transient response of the LESR signal of the PFO-C_{60} composite upon irradiation by light (450 nm) pulse. The data were recorded using the lower-field peak of the PFO signal (g_1) at 40 K.

posite and the comparison of action spectra between LESR and photocurrent seem to be interesting problems in order to clarify the charge-separation processes and the photogeneration of the polarons in more detail, which is beyond the main scope of the present work to investigate microscopic properties of polarons in PFO using magnetic resonance and is open for further studies.

Figure 7 shows the transient response of the LESR signal of the PFO-C_{60} composite upon irradiation by a light pulse (450 nm). The data were recorded using the lower-field peak of the PFO signal (g_1) with a microwave power of 0.06 mW at 40 K. The photoresponse is found to have two parts: a prompt part and a persistent one. That is, upon irradiation by light, the LESR signal increases rapidly then saturates. When irradiation ceases, the LESR signal decreases rapidly, and then the remaining part decreases very slowly. The prompt and persistent components are considered to be caused by shallow and deep traps in the PFO-C_{60} composite, respectively.[35,38] The decay time of the persistent component is on the order of several hours, which is extremely long compared with that of the prompt component. The behavior of the persistent component at low temperatures has been explained by nongeminate recombination of randomly distributed carriers using tunneling process assuming charge neutrality.[38,44] The intensity of the prompt decay component of LESR, I_{pr}, is defined as the difference between the LESR intensity under illumination and that at 30 min after the termination of irradiation. The intensity of the persistent decay component of LESR, I_{per}, is defined as the difference between the LESR intensity at 30 min after the termination of irradiation and that under dark conditions. The definition of I_{pr} and I_{per} is also shown in Fig. 7.

In the LESR studies of the composites,[38,44] steady-state conditions can be reached under light illumination (see Fig. 7); hence simple dependence of the LESR intensity on excitation-light intensity I_{ex} will give the information about the recombination process of the photogenerated charge carriers. The dependences of the twice-integrated LESR intensity on I_{ex} for the prompt and persistent LESR signals of the PFO-C_{60} composite are shown in Figs. 8(a) and 8(b), respectively. Here, N_h and N_e are the numbers of photogenerated

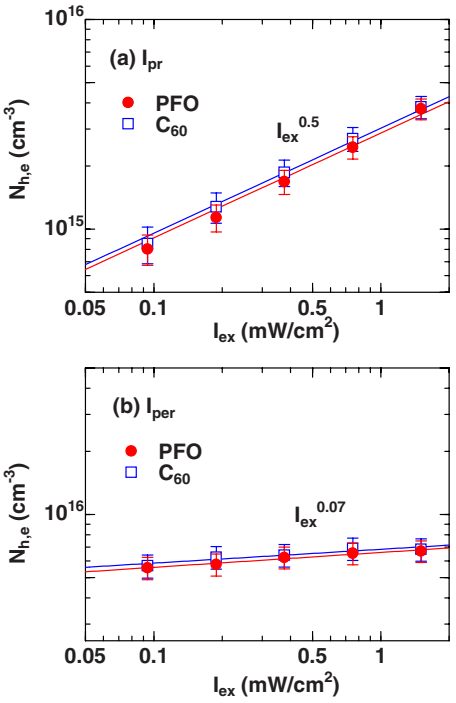

FIG. 8. (Color online) Dependences of the magnitude (in $\log_{10}$ base) of the LESR of the PFO-C_{60} composite on the excitation-light intensity I_{ex} at 60 K: the prompt components I_{pr} (a), and the persistent components I_{per} (b). Here, N_h and N_e are the numbers of photogenerated positive PFO polarons and photogenerated C_{60}^- radical anions per unit volume, respectively, which have been evaluated from the twice-integrated LESR intensity. The solid circles and open squares denote the signal intensities of PFO and C_{60}, respectively. Almost the same behavior for the I_{ex} dependence is also observed at 80 K.

positive PFO polarons and photogenerated C_{60}^- radical anions per unit volume, respectively, which have been evaluated by the twice-integrated LESR intensity. The solid circles and open squares denote the signal intensities of PFO (g_1) and C_{60} (g_2), respectively. These measurements were performed under 450 nm illumination at 40 K with a microwave power of 0.06 mW where no saturation occurs. The I_{pr} shows almost equal amounts of spins (i.e., almost equal twice-integrated ESR intensities) and increases monotonically as I_{ex} increases for both the low- and high-field LESR lines of PFO (g_1) and C_{60} (g_2). Both I_{pr} show an $I_{ex}^{0.5}$ power dependence within the light-power range 0.095–1.5 mW/cm^2. Almost the same behavior for the I_{ex} dependence is also observed at 80 K. This dependence ($I_{ex}^{0.5}$) implies bimolecular recombination (BR); similar results have been observed for the composites of a PPV derivative and a C_{60} derivative[21] and a regiorandom P3AT (RRa-P3AT)-C_{60} composite.[38] In contrast, I_{per} is nearly independent of the intensity of the previously applied light within the light-power range 0.095–1.5 mW/cm^2. This result is consistent with that of the composites of PPV derivative and C_{60} derivative[21] and the RR-P3AT-C_{60} composites,[35] which is related to the filling of deep-trap defect states present due to disorder in the PFO-C_{60} composite. Thus, in the following, we focus on the geminate recombination kinetics of charge carries in the time

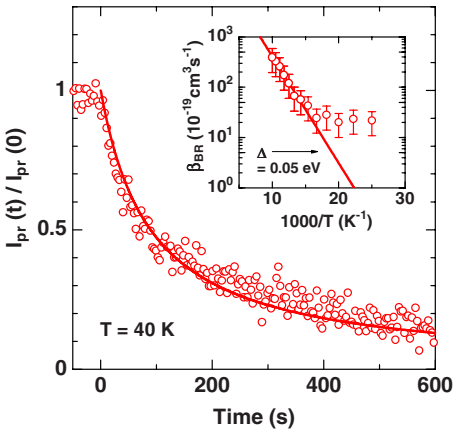

FIG. 9. (Color online) Decay of the prompt component of LESR I_{pr} for the PFO-C_{60} composite (C_{60}:5%) after the termination of 450 nm irradiation with $I_{ex} \sim 1.5$ mW/cm^2 at 40 K. The solid line shows the Eq. (2). Inset: Arrhenius plot of bimolecular-recombination (BR) rate constant β_{BR} of Eq. (2) for the PFO-C_{60} composite (C_{60}:5%), measured using 450 nm illumination.

regime of 100 ms–30 min that is related to the prompt component.

From the power dependence of the LESR intensities obtained above, we will discuss the rate constants of the BR of photogenerated charge carriers. Let β_{BR} be the rate constants of the BR, I the photon flux of excitation light per unit sample volume ($I \propto I_{ex}$), and Φ the generation efficiency of photocarriers, then we may write a phenomenological rate equation as

$$\frac{dN_{h,e}}{dt} = \Phi I - \beta_{BR} N_h N_e. \tag{1}$$

Because N_h and N_e are generated in pairs and equal to each other, we define the number N as $N=N_{h,e}$ that is evaluated from I_{pr} assuming the Curie law ($N \propto I_{pr}$), and use N from now on. We neglect the spatial variation in excitation density within the sample. Under a steady condition, N is expressed from Eq. (1) as $N=(\Phi I/\beta_{BR})^{0.5}$, which explains the data very well, as shown by the solid lines in Fig. 8(a).

This BR explains the transient decay of I_{pr} as presented below. Figure 9 shows the time dependence of the normalized I_{pr} for the PFO-C_{60} composite at 40 K under 450 nm illumination. The solid line in Fig. 9 represents the decay curves for BR derived from Eq. (1) under $I=0$ conditions as

$$\frac{N}{N_0} = (1 + \beta_{BR} N_0 t)^{-1}, \tag{2}$$

where N_0 is the number of polarons under steady-state condition. The experimental data are described with Eq. (2) very well using a temperature-dependent β_{BR}. Twice integrating the first-derivative LESR signal, we evaluate N_0 as 7.44×10^{15} cm^{-3} at 40 K, and then we evaluate β_{BR} at 40 K as 2.18×10^{-18} cm^3 s^{-1} by Eq. (2). The inset of Fig. 9 shows the temperature dependence of β_{BR} for the PFO-C_{60} composite in the form of the Arrhenius plot, which is related to the transport mechanism of photogenerated charge carriers. As temperature increases, the recombination becomes faster and β_{BR} becomes larger. The data below 75 K are almost independent of temperature, as also observed for the slow-decay component in the MDMO-PPV-PCBM composite[44] and the RR-P3AT-C_{60} composites,[38,41] indicating a tunneling process at low temperatures. On the other hand, the data above 75 K follow the activation-type formula $[\exp(-\Delta/kT)]$ as plotted by the solid line in the inset of Fig. 9, where the activation-energy Δ is evaluated as 0.05 eV. Therefore, the above results clearly show a crossover of the transport mechanism from hopping to tunneling with decrease in temperature. It is interesting to note that the above activation energy is close to that of 0.06 eV reported for a composite of a PPV derivative (MEH-PPV: poly[2-methoxy,5-(2′-ethyl-hexyloxy)-*p*-phenylene vinylene]) and C_{60}.[18] Therefore, the present Δ is reasonably ascribed to the hopping energy of shallowly trapped polarons causing the prompt component of the LESR.

It should be noted that a novel phenomenon considering quadrimolecular recombination (QR) of photogenerated charge carriers has been found in the RR-P3AT-C_{60} composites,[38,41] where two positive polarons and two C_{60}^- radical anions recombine simultaneously. On the other hand, only BR phenomena have been found in the PFO-C_{60} composite in addition to the usual composites including the RRa-P3AT-C_{60} composite.[38] As discussed in the previous works,[38,41] the QR phenomenon is probably related to the high-carrier mobilities leading to the formation of doubly charged states, either bipolarons or polaron pairs on the polymer chains, which is also supported by the present result of the PFO-C_{60} composite because carrier mobility in PFO is reported to be much lower than that of RR-P3AT.[45] It should be also noted that recent ESR studies of metal-insulator-semiconductor (MIS) diodes and transistors of RR-P3AT have indicated the occurrence of such spinless-doubly-charged states through the observation of spin-saturation phenomena for higher concentrations of field-injected charges.[46–49]

C. LENDOR of the PFO-C_{60} composite

ENDOR is a powerful method to determine the wave function (spin distribution) of the polarons by studying the proton-hyperfine coupling to the polaron spin on the conjugated chain, as shown in the studies of PPV (Ref. 26) and RR-P3AT (Ref. 37); ENDOR is a more direct method than ESR. However, the ENDOR method needs larger number of spins to detect the signal compared with ESR method, and is not capable of detecting the signal of pure PFO because of its low-spin concentration. This difficulty has been overcome by utilizing the present PFO-C_{60} composite because of the high photogeneration efficiency of polarons mentioned above.

Figure 10 shows the frequency-derivative LENDOR spectra of the PFO-C_{60} composite at 4 K. The data were recorded with a microwave power of 2 mW and an rf power setting of −3 dB of the Bruker ENDOR unit under 450 nm (~2.8 eV) illumination where the enhancement of the LESR signals occurs (see Fig. 4). Solid and dotted lines represent the spectra of PFO and C_{60}, which are obtained by using

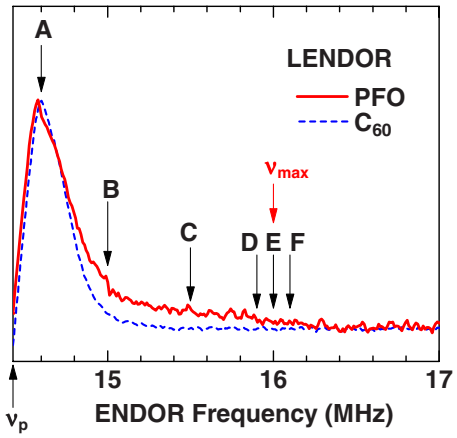

FIG. 10. (Color online) Frequency-derivative LENDOR spectra of the PFO-C_{60} composite (C_{60}:5%) at 4 K under 450 nm (~2.8 eV) illumination for the frequency region higher than the free-proton frequency ν_p=14.45 MHz. Solid and dotted lines represent the spectra of PFO and C_{60}, which are obtained by using the resonance magnetic fields of the LESR signals of positive polarons in PFO (g_1=2.003) and radical-anions C_{60}^- (g_2=1.999) shown in Fig. 4, respectively. ν_{max} represents the maximum ENDOR shift in the PFO signal corresponding to the maximum hyperfine-tensor component. Position *A*-*F* shows the frequencies at which LENDOR-induced ESR are shown in Fig. 11.

resonance magnetic fields of the LESR signals of PFO (g_1 =2.003) and C_{60} (g_2=1.999) shown in Fig. 4, respectively. In Fig. 10, the frequency region higher than the free-proton frequency ν_p=14.45 MHz is shown because the spectra are almost symmetrical around ν_p. A remarkable feature of the LENDOR spectrum of PFO is a broad distribution of the spectral frequency up to ~16 MHz, which directly shows the spin-density distribution of the photogenerated polarons on the polymer chain as discussed below.[26,28,37] A finite spin-density ρ on a carbon $p\pi$ orbital causes a hyperfine coupling with the proton bonded to the carbon with the magnitude of $\rho\boldsymbol{A}$.[28,37] Here $\boldsymbol{A}$ is the hyperfine tensor of a π electron due to the C-H proton. The principal axes of the hyperfine coupling are shown in Fig. 1(a), where the x and z axes are parallel to the C-H bond and $p\pi$ orbital, respectively. The tensor becomes diagonal in the above coordinate system and the principal components are given as $A_{xx}=-(1-\alpha_{\text{aniso}})A$, $A_{yy}=-(1+\alpha_{\text{aniso}})A$, and $A_{zz}=-A$. Here A is the so-called McConnell's constant with the magnitude of 56–84 MHz in the frequency unit. We adopt a typical value of A=70 MHz in the following analysis.[28,37] $\alpha_{\text{aniso}}\sim 0.5$ represents the relative magnitude of the anisotropic coupling. Let $l_i(i=x,y,z)$ be the direction cosines of the external magnetic field to the hyperfine axes for a proton bonded to a particular carbon site with a spin-density ρ; then we may write the ENDOR frequency as

$$\nu_{\pm} = \sqrt{\sum_i \left(\nu_p \pm \frac{1}{2}\rho A_{ii}\right)^2 l_i^2}, \tag{3}$$

where $\pm$ represent the two branches of the ENDOR frequency.[50] Therefore, the distribution of ρ of the photogenerated polarons causes the broad distribution of the LENDOR spectral frequency as shown in Fig. 10. The spectrum of PFO has weak structure, as observed for RR-P3AT,[37,40] compared with that of PPV.[26] This indicates that the magnitude of ρ on the PFO chain has a monotonically decaying distribution (ρ on the PPV chain distributes nonmonotonically with the maximum spin density at vinyl sites).[29,30] On the other hand, the narrower linewidth of the LENDOR signal of C_{60}^- is reasonably ascribed to the absence of hyperfine coupling from C_{60} carbon sites because of the lack of protons in the C_{60} molecule. Then the signal is ascribed to electron-nuclear dipolar coupling due to protons in the main chain or in alkyl side chains of PFO adjacent to C_{60} molecules, that is, the so-called matrix protons. From the observed narrow linewidth, the mean distance between C_{60} and adjacent protons is evaluated as several Å.

The observable ρ for PFO is related to carbons with C-H bonds (β carbons), not the carbons linking the adjoining phenyl rings (α carbon) nor carbons in the alkyl side chain (β' carbons) [see the definition in Fig. 1(a)]. From now on, we will define the maximum spin density on α and β carbons as $\rho_{\alpha,\max}$ and $\rho_{\beta,\max}$, respectively. The spin density on the β' carbon is considered to be almost the same as that on the β carbon because the alkyl side chain has no π electrons. In this context, hyperfine coupling from protons on the side chain would be negligible in the first approximation.

In order to determine the spatial extent of the photogenerated polarons, we need to obtain $\rho_{\beta,\max}$ because $\rho_{\beta,\max}$ is nearly inversely proportional to the full width at the half maximum of the spin distribution, that is, the spatial extent of the spin species.[1,28,37,40,51] We can obtain $\rho_{\beta,\max}$ directly from the experimental results as follows. When the direction of the external magnetic field is parallel to one of the principal axes of the hyperfine tensor, then Eq. (3) reduces to

$$\nu_{\pm} = \left|\nu_p \pm \frac{1}{2}\rho A_{ii}\right|, \quad \text{for } i=x,y,z. \tag{4}$$

The second term of the right-hand side shows the frequency shift due to the hyperfine field and $\pm$ sign corresponds to up and down-spin orientations. Thus the maximum ENDOR frequency $\nu_{\beta,\max}$ is given as $\nu_p+(1/2)\rho_{\beta,\max}|A_{yy}|$ because A_{yy} has the largest absolute magnitude among the hyperfine-tensor components. Therefore, it is essential to confirm the slowly varying line shape of the LENDOR spectrum of PFO shown in Fig. 10 in order to determine $\nu_{\beta,\max}$ (or $\rho_{\beta,\max}$), otherwise the possibility of line-shape distortion due to the background deviation is not excluded. The ENDOR-induced ESR technique is especially suitable for this purpose, and has been successfully applied to studies of the polarons in PPV[26] and RR-P3AT,[37,40] and of the solitons in polyacetylene.[52] In this method, the frequency of rf wave for the ENDOR transition is fixed at a particular value and then the ENDOR intensity is recorded as a function of the external magnetic field. This provides the ESR spectrum of the spin species giving rise to the ENDOR signal at the given frequency. Thus ENDOR-induced ESR can trace the intrinsic ENDOR line shape by examining whether ENDOR-induced ESR signal can be detected for the wing region of the ENDOR spectrum.

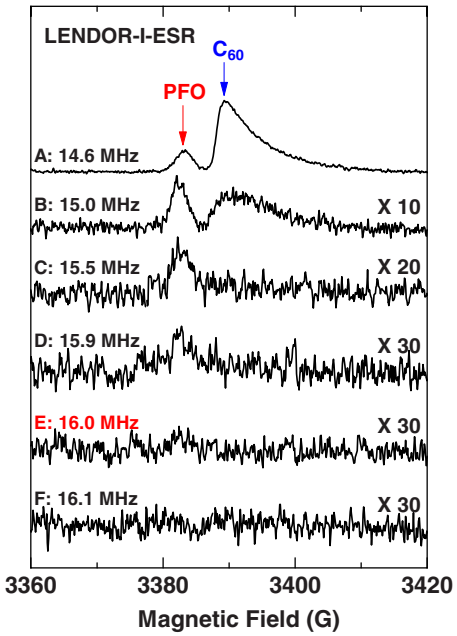

FIG. 11. (Color online) LENDOR-induced ESR signals of the PFO-C_{60} composite (C_{60}:5%) at 4 K under 450 nm illumination. Each signal is measured at the ENDOR frequencies shown in Fig. 10 as *A* (14.6 MHz), *B* (15.0 MHz), *C* (15.5 MHz), *D* (15.9 MHz), *E* (16.0 MHz), and *F* (16.1 MHz), respectively.

The LENDOR-induced ESR signals of the PFO-C_{60} composite at 4 K under 450 nm illumination are shown in Fig. 11. Each signal is measured at the ENDOR frequencies shown in Fig. 11 as *A* (14.6 MHz), *B* (15.0 MHz), *C* (15.5 MHz), *D* (15.9 MHz), *E* (16.0 MHz), and *F* (16.1 MHz), respectively. At 14.6 MHz (*A*), two signals of PFO and C_{60} are observed because the ENDOR signals of PFO and C_{60} coexist at 14.6 MHz (see Fig. 10). On the other hand, a single signal due to the photogenerated polarons of PFO is observed at 15.5 MHz (*C*), which is consistent with the absence of ENDOR signal of C_{60} at above 15.5 MHz (see Fig. 10). The signal of PFO is also observed at 15.9 MHz (*D*) and 16.0 MHz (*E*) although the signal intensity is weak. With this method $\nu_{\beta,\max}=16.0$ MHz was determined. Therefore, $\rho_{\beta,\max}=0.032$ is obtained using the above formulas of $\nu_{\beta,\max}=\nu_p+(1/2)\rho_{\beta,\max}|A_{yy}|$. This value can be compared with the theoretical result, which will be presented below.

D. Spatial extent of polarons in PFO

In this subsection, we present the theoretically calculated spin-density distribution of a polaron in PFO and its ESR spectrum calculated using this spin-density distribution. The theoretical results are compared with the experimentally determined spin density as well as the observed ESR spectra for PFO and the PFO-C_{60} composite.

Our theoretical model is the PPP model[50,53–55] for π electrons and the unrestricted Hartree-Fock approximation is applied to it. This model contains the long-range electron-electron interaction as well as electron-lattice coupling. The details of parameters used in this model, such as the transfer integral, the electron-lattice coupling constant, and Coulomb

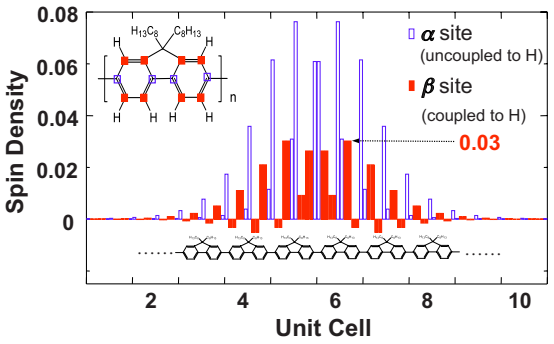

FIG. 12. (Color online) Theoretical spin-density distribution of a polaron in PFO, obtained by the Pariser-Parr-Pople model. Filled and open bars show the spin densities at the carbon sites coupled (β site) and uncoupled (α site) to protons in poly(*p*-phenylene), respectively. Since the π-electron network is the same between PFO and poly(*p*-phenylene) as a first approximation, the actual calculation is performed for a poly(*p*-phenylene) chain ignoring the side alkyl chains.

interactions, have been described in the literature.[50] Since π conjugation does not extend to the alkyl side chains in the PFO structure, we can ignore them, as a first approximation. Therefore, in the present study, the spin density of a polaron has been calculated using a single chain of poly(*p*-phenylene), instead of PFO, with 120 carbon sites. In addition, we assume a planar geometry of the molecule. Reference 56 has reported that a completely flat conformation reproduces the observed ultraviolet photoelectron spectroscopy (UPS) spectrum of PFO much better than a geometry with a torsion angle of 40°, which is probably ascribed to solid-state packing effects forcing the polymer backbone to be planar.

Figure 12 shows theoretically calculated spin-density distribution of a positively charged polaron. Filled and open bars show the spin densities at the carbon sites coupled (β site) and uncoupled (α site) to protons in the poly(*p*-phenylene) structure. Here, we do not distinguish β and β' sites in the figure. One of the characteristic features in this spin-density distribution is that the spin densities at the β sites are roughly half of those at the α sites in each molecular unit. The maximum spin density among the β sites is obtained as 0.03, which agrees with the aforementioned experimental result of 0.032 for β sites very well. As shown by the figure, the spatial extent of the polaron, i.e., the full width at half maximum of the spin-density distribution, is evaluated as ~3 unit cells of PFO. This extension corresponds to ~36 carbon atoms in the π system, not including the other carbons, which is on the same order of the spatial extent of a polaron in other polymers: ~32 atoms for PPV (~4 unit cells)[26–32] and ~40 atoms for RR-P3AT (~10 unit cells).[37,40]

Figure 13 shows the calculated ESR spectra (solid lines) in first-derivative form (upper figure) and in integrated form (lower figure), respectively, using the theoretical spin-density distribution shown in Fig. 12. The parameters employed in the calculation of the spectra are the same as those reported previously.[27,28,30,50] In this calculation, the absence of protons at β' sites are considered by neglecting the hyperfine

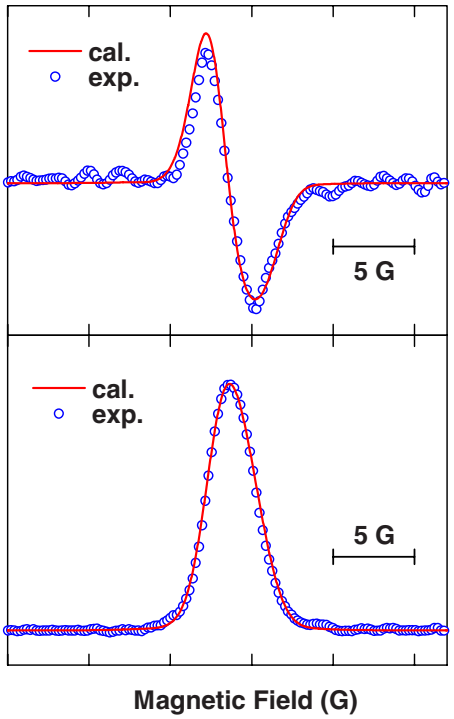

FIG. 13. (Color online) Calculated ESR spectra (solid lines) and experimental LESR spectra (circles) of PFO, in first derivative form (upper figure) and in integrated form (lower figure). The theoretical spin-density distribution shown in Fig. 12 is used for the calculated spectra.

interaction at these sites. The experimental results of the LESR spectra of the pure PFO are also plotted as circles in each figure, which were obtained at 10 K under 300 nm illuminations. The calculated spectra and linewidths explain the experimental data very well: The peak-to-peak linewidth ΔH_{pp} in the upper figure is estimated as 3.0 G for the calculated spectrum; the experimentally obtained ΔH_{pp} is 3.0 G. The full width at half maximum of linewidth $\Delta H_{1/2}$ in the lower figure is calculated as 3.5 G; the experimentally obtained $\Delta H_{1/2}$ is 3.4 G.

The calculated ESR spectrum is also compared with the LESR spectrum of the PFO-C_{60} composite in Fig. 14. The data were measured at 10 K under 450 nm illuminations. In this case, the calculated spectrum explains the experimental data well in a lower magnetic field region below the resonance magnetic field indicated by the g_1 value, where the LESR signal of PFO is not overlapped with that of C_{60} in the experimental LESR spectrum. Thus, the theoretically calculated spin-density distribution shown in Fig. 12 reproduces the experimentally obtained LESR spectra very well.

The LESR linewidth is narrower in PFO than in PPV: In PFO, the spin densities at the β sites contribute to ESR linewidth owing to hyperfine interaction with protons. Meanwhile, in PPV, the spin densities at the vinyl carbons also contribute and the maximum magnitude among them is evaluated to be ca. 0.09.[26,30,50,57]

IV. SUMMARY

The PFO and its composite with C_{60} have been investigated by means of the light-induced ESR (LESR) and light-induced ENDOR (LENDOR) methods using variable photoexcitation energy up to 4.1 eV. For pure PFO, the LESR signal due to photogenerated polarons is observed below 60 K. Its excitation spectrum shows a clear enhancement at above ~3.7 up to 4.1 eV, which is consistent with the enhancement of photocurrent at above ~3.6 eV and indicates the photogeneration of polarons. For the PFO-C_{60} composite, two LESR signals are observed, which are ascribed to photogenerated positive polarons on PFO and radical-anions C_{60}^- owing to the photoinduced electron transfer from PFO to C_{60}, respectively. A significant enhancement of the LESR signals is observed in the excitation spectrum at around 2.8 eV. Prompt and persistent LESR signal components are observed, and the excitation-light intensity I_{ex} dependence shows that the prompt contribution increases monotonically as I_{ex} increases while the persistent contribution is found to be independent of I_{ex} due to filling of deep traps. The dependences of the prompt LESR component on I_{ex} and time are well explained by the bimolecular recombination of photogenerated carriers in the composite. The LENDOR and LENDOR-induced ESR studies have evaluated the maximum spin density of a polaron on the carbon sites coupled to the protons in PFO chains as 0.032, which is well reproduced by the theoretical calculation based on the PPP model. The experimental LESR signals of PFO are also well reproduced by using the calculated spin-density distribution, which evaluates the spatial extent of polarons in PFO as ~3 unit cells.

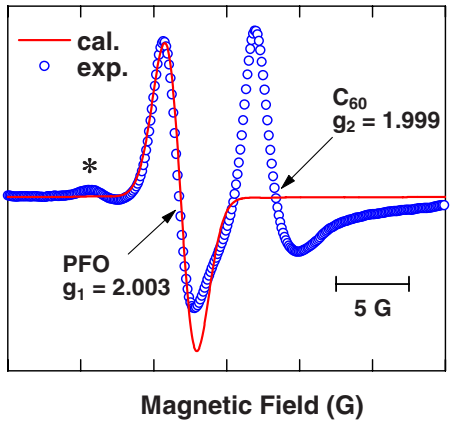

FIG. 14. (Color online) Calculated ESR spectrum (solid line) of PFO and experimental LESR spectrum (circles) of the PFO-C_{60} composite (C_{60}:5%) in first derivative. The theoretical spin-density distribution shown in Fig. 12 is used for the calculated spectrum. The weak signal in the lower magnetic field region denoted by an asterisk (*) is the spin-flip transition mentioned in Fig. 4.

ACKNOWLEDGMENTS

We would like to thank T. Ohnishi for supplying PFO materials. This work was partially supported by Grants-in-Aid for Scientific Research (Grants No. 18686002 and No. 17340094) and for Science Research in a Priority Area "Super-Hierarchical Structures" (Grants No. 17067007 and No. 17067018) from the Ministry of Education, Culture, Sports, Science and Technology of Japan.

*Present address: Institute of Materials Science, University of Tsukuba, Tsukuba, Ibaraki 305-8573, Japan; marumoto@ims.tsukuba.ac.jp

[1] A. J. Heeger, S. Kivelson, J. R. Schrieffer, and W.-P. Su, Rev. Mod. Phys. **60**, 781 (1988).
[2] *Conjugated Conducting Polymers*, Springer Series in Solid-State Sciences Vol. 102, edited by H. G. Kiess (Springer, Berlin, Heidelberg, 1992).
[3] F. H. Friend, R. W. Gymer, A. B. Holmes, J. H. Burroughes, R. N. Marks, C. Taliani, D. D. C. Bradley, D. A. Dos Santos, J. L. Brédas, M. Lögdlund, and W. R. Salaneck, Nature (London) **397**, 121 (1999).
[4] A. W. Grice, D. D. C. Bradley, M. T. Bernius, M. Inbasekaran, W. W. Wu, and E. P. Woo, Appl. Phys. Lett. **73**, 629 (1998).
[5] N. C. Greenham, I. D. W. Samuel, G. R. Hayes, R. T. Phillips, Y. A. R. R. Kessener, S. C. Moratti, A. B. Holmes, and R. H. Friend, Chem. Phys. Lett. **241**, 89 (1995).
[6] S. Janietz, D. D. C. Bradley, M. Grell, C. Giebeler, M. Inbasekaran, and E. P. Woo, Appl. Phys. Lett. **73**, 2453 (1998).
[7] A. J. Cadby, P. A. Lane, H. Mellor, S. J. Martin, M. Grell, C. Giebeler, D. D. C. Bradley, M. Wohlgenannt, C. An, and Z. V. Vardeny, Phys. Rev. B **62**, 15604 (2000).
[8] L. S. Liao, M. K. Fung, C. S. Lee, S. T. Lee, M. Inbasekaran, E. P. Woo, and W. W. Wu, Appl. Phys. Lett. **76**, 3582 (2000).
[9] D. Y. Kim, H. N. Cho, and C. Y. Kim, Prog. Polym. Sci. **25**, 1089 (2000).
[10] M. Ariu, D. G. Lidzey, M. Lavrentiev, D. D. C. Bradley, M. Jandke, and P. Strohriegl, Synth. Met. **116**, 217 (2001).
[11] J. J. M. Halls, C. A. Walsh, N. C. Greenham, E. A. Marseglia, R. H. Friend, S. C. Moratti, and A. B. Holmes, Nature (London) **376**, 498 (1995).
[12] S. Morita, A. A. Zakhidov, and K. Yoshino, Solid State Commun. **82**, 249 (1992).
[13] N. S. Sariciftci, L. Smilowitz, A. J. Heeger, and F. Wudl, Science **258**, 1474 (1992).
[14] K. Yoshino, S. Morita, T. Kawai, H. Araki, X. H. Yin, and A. A. Zakhidov, Synth. Met. **56**, 2991 (1993).
[15] K. Yoshino, X. H. Yin, S. Morita, T. Kawai, and A. A. Zakhidov, Solid State Commun. **85**, 85 (1993).
[16] L. Smilowitz, N. S. Sariciftci, R. Wu, C. Gettinger, A. J. Heeger, and F. Wudl, Phys. Rev. B **47**, 13835 (1993).
[17] G. Yu, J. Gao, J. C. Hummelen, F. Wudl, and A. J. Heeger, Science **270**, 1789 (1995).
[18] S. B. Lee, A. A. Zakhidov, I. I. Khairullin, V. Yu. Sokolov, P. K. Khabibullaev, K. Tada, K. Yoshimoto, and K. Yoshino, Synth. Met. **77**, 155 (1996).
[19] E. S. Maniloff, D. Vacar, D. W. McBranch, H.-L. Wang, B. R. Mattes, J. Gao, and A. J. Heeger, Opt. Commun. **141**, 243 (1997).
[20] E. K. Miller, K. Lee, K. Hasharoni, J. C. Hummelen, F. Wudl, and A. J. Heeger, J. Chem. Phys. **108**, 1390 (1998).
[21] V. Dyakonov, G. Zoriniants, M. Scharber, C. J. Brabec, R. A. J. Janssen, J. C. Hummelen, and N. S. Sariciftci, Phys. Rev. B **59**, 8019 (1999).
[22] C. J. Brabec, S. Sariciftci, and J. C. Hummelen, Adv. Funct. Mater. **11**, 15 (2001).
[23] S. E. Shaheen, C. J. Brabec, N. S. Sariciftci, F. Padinger, T. Fromherz, and J. C. Hummelen, Appl. Phys. Lett. **78**, 841 (2001).
[24] C. J. Brabec, G. Zerza, G. Cerullo, S. DeSilvestri, S. Luzzati, J. C. Hummelen, and N. S. Sariciftci, Chem. Phys. Lett. **340**, 232 (2001).
[25] Q.-H. Xu, D. Moses, and A. J. Heeger, Phys. Rev. B **67**, 245417 (2003).
[26] S. Kuroda, T. Noguchi, and T. Ohnishi, Phys. Rev. Lett. **72**, 286 (1994).
[27] S. Kuroda, K. Murata, T. Noguchi, and T. Ohnishi, J. Phys. Soc. Jpn. **64**, 1363 (1995).
[28] S. Kuroda, Int. J. Mod. Phys. B **9**, 221 (1995).
[29] S. Kuroda, K. Murata, Y. Shimoi, S. Abe, T. Noguchi, and T. Ohnishi, in *Materials and Measurements in Molecular Electronics*, Springer Proceedings in Physics 81 edited by K. Kajimura and S. Kuroda, (Springer, Tokyo, 1996), p. 256.
[30] S. Kuroda, K. Marumoto, H. Ito, N. C. Greenham, R. H. Friend, Y. Shimoi, and S. Abe, Chem. Phys. Lett. **325**, 183 (2000).
[31] S. Kuroda, K. Marumoto, N. C. Greenham, R. H. Friend, Y. Shimoi, and S. Abe, Synth. Met. **119**, 655 (2001).
[32] S. Kuroda, K. Marumoto, Y. Shimoi, and S. Abe, Thin Solid Films **393**, 304 (2001).
[33] S. Kuroda, K. Marumoto, N. C. Greenham, R. H. Friend, Y. Shimoi, and S. Abe, Mol. Cryst. Liq. Cryst. **371**, 159 (2001).
[34] K. Marumoto, N. Takeuchi, S. Kuroda, R. Azumi, and M. Matsumoto, Synth. Met. **119**, 549 (2001).
[35] K. Marumoto, N. Takeuchi, T. Ozaki, and S. Kuroda, Synth. Met. **129**, 239 (2002).
[36] K. Marumoto, Y. Muramatsu, N. Takeuchi, and S. Kuroda, Synth. Met. **135-136**, 433 (2003).
[37] K. Marumoto, N. Takeuchi, and S. Kuroda, Chem. Phys. Lett. **382**, 541 (2003).
[38] K. Marumoto, Y. Muramatsu, and S. Kuroda, Appl. Phys. Lett. **84**, 1317 (2004).
[39] K. Marumoto, T. Sakamoto, Y. Muramatsu, and S. Kuroda, Synth. Met. **154**, 85 (2005).
[40] S. Kuroda, K. Marumoto, T. Sakanaka, N. Takeuchi, Y. Shimoi, S. Abe, H. Kokubo, and T. Yamamoto, Chem. Phys. Lett. **435**, 273 (2007).
[41] H. Tanaka, N. Hasegawa, T. Sakamoto, K. Marumoto, and S. Kuroda, Jpn. J. Appl. Phys. **46**, 5187 (2007).
[42] K. Marumoto, T. Sakamoto, S. Watanabe, H. Ito, and S. Kuroda, Jpn. J. Appl. Phys. **46**, L1191 (2007).
[43] K. Marumoto, S. Kuroda, T. Takenobu, and Y. Iwasa, Phys. Rev. Lett. **97**, 256603 (2006).
[44] N. A. Schultz, M. C. Scharber, C. J. Brabec, and N. S. Sariciftci, Phys. Rev. B **64**, 245210 (2001).
[45] Y. Naito, OYO BUTURI **73**, 924 (2004).
[46] K. Marumoto, Y. Muramatsu, S. Ukai, H. Ito, and S. Kuroda, J. Phys. Soc. Jpn. **73**, 1673 (2004).
[47] K. Marumoto, Y. Muramatsu, Y. Nagano, T. Iwata, S. Ukai, H. Ito, S. Kuroda, Y. Shimoi, and S. Abe, J. Phys. Soc. Jpn. **74**, 3066 (2005).
[48] S. Watanabe, K. Ito, H. Tanaka, H. Ito, K. Marumoto, and S. Kuroda, Jpn. J. Appl. Phys. **46**, L792 (2007).
[49] H. Tanaka, S. Watanabe, H. Ito, K. Marumoto, and S. Kuroda, Appl. Phys. Lett. **94**, 103308 (2009).
[50] Y. Shimoi, S. Abe, S. Kuroda, and K. Murata, Solid State Commun. **95**, 137 (1995).
[51] K. Yonemitsu, Y. Ono, and Y. Wada, J. Phys. Soc. Jpn. **57**, 3875 (1988).
[52] S. Kuroda and H. Shirakawa, Phys. Rev. B **35**, 9380 (1987).

[53] R. Pariser and R. G. Parr, J. Chem. Phys. **21**, 466 (1953).
[54] R. Pariser and R. G. Parr, J. Chem. Phys. **21**, 767 (1953).
[55] J. A. Pople, Trans. Faraday Soc. **49**, 1375 (1953).
[56] G. Greczynski, M. Fahlman, W. R. Salaneck, N. Johansson, D. A. dos Santos, A. Dkhissi, and J. L. Brédas, J. Chem. Phys. **116**, 1700 (2002).
[57] S. Kuroda, Y. Shimoi, S. Abe, T. Noguchi, and T. Ohnishi, J. Phys. Soc. Jpn. **67**, 3936 (1998).